Level structure of ^{83}Zr

U. J. Hüttmeier, C. J. Gross, D. M. Headly,* E. F. Moore, and S. L. Tabor
Department of Physics, Florida State University, Tallahassee, Florida 32306

T. M. Cormier and P. M. Stwertka
Nuclear Structure Laboratory, University of Rochester, Rochester, New York 14627

W. Nazarewicz
Supercomputer Computations Research Institute, Florida State University, Tallahassee, Florida 32306
and Institute of Physics, Warsaw Institute of Technology, PL-00662 Warsaw, Poland
(Received 2 September 1987)

The level structure of ^{83}Zr was investigated via the fusion-evaporation reaction ^{54}Fe(^{32}S,2pn)^{83}Zr at beam energies between 105 and 120 MeV using in-beam γ-ray spectroscopy techniques. γ transitions from the decay of ^{83}Zr were unambiguously identified by means of recoil-γ, neutron-γ, and x-ray-γ coincidences. The decay scheme was constructed on the basis of Compton suppressed γ-γ coincidences, delayed γ-γ coincidences, and angular distribution measurements. A total of 34 transitions were identified connecting 26 new energy levels and the previously known ground state. The lifetimes of two low-lying isomeric states were determined. A decoupled positive parity band built on the odd $g_{9/2}$ neutron configuration was observed up to spin $\frac{37}{2}\hbar$ with the first band crossing due to proton alignment showing a sharp backbend at $\hbar\omega=0.5$ Mev. A strongly coupled negative parity band based on a $\frac{5}{2}^-$ bandhead was observed up to spin $\frac{35}{2}\hbar$. The angular momentum alignment is discussed and compared to neighboring nuclei. A theoretical analysis was performed using the Woods-Saxon cranking model. The results of the calculation are consistent with the experimental findings for ^{83}Zr and its neighbors. Triaxial shapes are predicted for all observed bands in ^{83}Zr. At higher angular momenta a transition to well-deformed prolate bands involving the $h_{11/2}$ intruder orbitals is expected.

I. INTRODUCTION

The systematic study of nuclei in the mass $A\approx 80$ region has revealed a wide variety of collective behavior. Rather strongly deformed prolate and oblate shapes often coexist with nearly spherical shapes. Other nuclei are soft, showing considerable changes in shape and deformation with only a small variation in the particle number or occupied orbitals. Improved experimental techniques have revealed a new region of strong deformation among the neutron deficient Kr and Sr nuclei.[1,2] Very recent work[3] indicates that this region of strong deformation extends to the light Zr isotopes.

The ^{84}Zr nucleus has recently been observed[4] up to spin $34\hbar$, the highest spin presently known in the $A\approx 80$ mass region. The ground state displays the characteristics of a spherical shape coexisting with a triaxial deformation.[5] With increasing rotational frequency, however, the triaxial deformation quickly becomes energetically more favorable.[5] In the neighboring ^{82}Zr isotope[3] the prolate deformation is energetically favored over the weakly deformed oblate shape (see Sec. IV). On the other hand, there is no information in the literature on the structure of the light odd Zr isotopes. The study of these odd nuclei is important because they provide an experimental probe of the neighboring deformation-soft even-even cores. The low energy structure in particular gives information on the properties of the involved quasiparticle configurations.

The present work is an experimental and theoretical investigation of the level structure of ^{83}Zr. At the beginning of this investigation only the results from β decay studies[6-12] with tentative spin and parity assignments for the ground state were available in the literature. No information on excited states of ^{83}Zr had been published, although we have since learned of unpublished work[13] on this nucleus.

Due to the lack of previous information, particular care was taken to identify the γ transitions from the decay of excited states in ^{83}Zr and to construct the low energy level scheme. The experimental techniques and results are contained in Sec. II and the construction of the level scheme is discussed in Sec. III. A comparison between the collective properties of neighboring even-even Sr and Zr isotopes is presented in Sec. IV. A cranking shell model analysis is given in Sec. V. In Sec. VI the experimental findings are compared to Woods-Saxon-Bogolyubov cranking calculations. Some of the results of the present work were previously reported in Ref. 14.

II. EXPERIMENTAL TECHNIQUES AND RESULTS

In all experiments presented in this section, high spin states in ^{83}Zr were populated via the reaction

^{54}Fe(^{32}S,2pn)^{83}Zr at beam energies between 105 and 120 MeV. The particle decay of the compound nucleus in the above heavy ion reaction populates excited states in a large number of residual nuclei. γ rays from the decay of excited states in $A=83$ reaction products were identified by means of recoil-γ and γ-γ coincidence experiments performed at the Nuclear Structure Laboratory at the University of Rochester. A subsequent neutron-γ coincidence experiment was performed at Florida State University. The results of the two particle-γ coincidence experiments in combination with x-ray-γ coincidences (Sec. II D) allowed an unambiguous identification of the transitions in ^{83}Zr.

All other experiments, including additional γ-γ coincidence measurements, were performed at Florida State University (FSU) with 105–115 MeV ^{32}S beams from the FSU Super FN Tandem, using a second stripper midway down the high energy column[15] to provide the necessary boost. The placement of transitions in the level scheme at high spin was established with the help of Compton suppressed and multiplicity filtered γ-γ coincidences. The low energy structure of ^{83}Zr was constructed on the basis of delayed γ-γ coincidences, using a low energy photon spectrometer. Spin assignments were based on angular distribution measurements and, in the case of the two lowest energy transitions, on internal conversion and transition probability arguments.

A. Recoil-γ coincidences

In order to identify the mass of the γ-decaying nucleus, the reaction products were separated with the Rochester recoil mass spectrometer[16] (RMS). Recoils were detected at the focal plane of the RMS in a planar 15×70 mm position sensitive silicon detector. The thin target of 200 μg/cm^2 97% enriched ^{54}Fe evaporated on a 20 μg/cm^2 ^{12}C foil was bombarded with a ^{32}S beam of 120 MeV. Parameters of the RMS were adjusted to focus mass $A=82$ and $A=83$ nuclei simultaneously onto the focal plane detector.

The γ rays in coincidence with the recoiling nuclei were detected in five high efficiency germanium detectors (all 23% or better) positioned at $\pm90°$, $\pm150°$, and 30° with respect to the beam direction. The γ spectra in coincidence with mass 83 nuclei were Doppler-shift corrected and added together. The sum spectrum is shown in the upper half of Fig. 1.

B. Neutron-γ coincidences

A neutron-γ coincidence experiment was performed in order to distinguish γ rays from the decay of ^{83}Zr and ^{83}Y. The reaction populates ^{83}Zr via 2pn evaporation from the compound nucleus ^{86}Mo, while ^{83}Y, the strongest reaction product, is populated via 3p evaporation. Other mass $A=83$ reaction products (^{83}Nb or ^{83}Mo) are too far from the valley of β stability to have any appreciable cross section in the present reaction. [Evaporation model calculations (e.g., cascade[17]) predict negligible yields for the 2np and 3n evaporation channels.]

A 1 mg/cm^2 ^{54}Fe target was bombarded with a 105 MeV ^{32}S beam. γ rays were detected in a Compton suppressed intrinsic Ge detector with 25% efficiency positioned at 90° to the beam direction. Neutrons were detected in an NE213 liquid scintillator positioned very close to the target at 0°. Pulse shape discrimination was used to separate neutrons from γ rays in the scintillator.

The neutron gated γ spectrum is shown in Fig. 1 together with the mass $A=83$ gated γ spectrum. The combination of the two coincidence spectra allows the

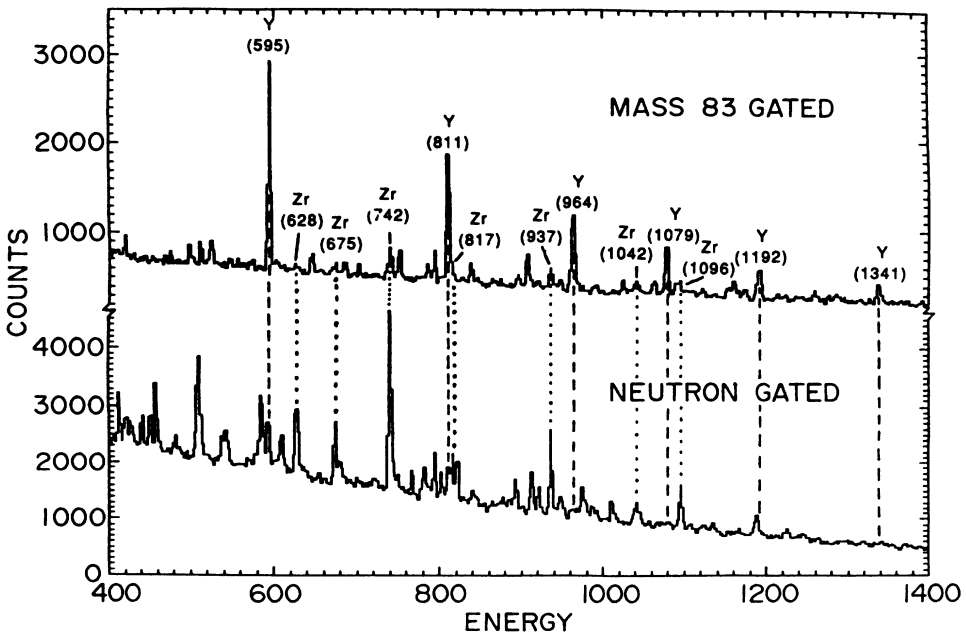

FIG. 1. The spectrum of γ rays in coincidence with mass 83 recoils separated with the Rochester recoil mass spectrometer (top) and the corresponding spectrum in coincidence with neutrons (bottom).

TABLE I. Energies, relative intensities, angular distribution coefficients, mixing ratios or multipolarities, spin assignments, and initial level energies for γ transitions in ^{83}Zr observed in the ^{54}Fe(^{32}S,2pn)^{83}Zr reaction at 110 MeV. Intensities are tabulated as the A_0 coefficient of the angular distribution and are normalized to the 741.5 keV transition. An intensity estimate at 60° is given where angular distribution coefficients could not be obtained. Error estimates in the last digits are given in parentheses.

E_γ (keV)	Relative intensity	A_2/A_0	A_4/A_0	δ or Multipol.	$I_i \rightarrow I_f$	E_{level} (keV)
24.3[a]	265(75)			$E1$	$\frac{7}{2}^+ \rightarrow \frac{5}{2}^-$	77.0
52.7[b]	385(45)			$E2$	$\frac{5}{2}^- \rightarrow \frac{1}{2}^-$	52.7
61.7[c]	225(32)	−0.41(2)	0.00(2)	0.05	$\frac{9}{2}^+ \rightarrow \frac{7}{2}^+$	138.7
111.2	2(1)	−0.35(9)	0.04(9)	0.04	$\frac{13}{2}^+ \rightarrow \frac{11}{2}^+$	880.2
261.5	7(2)	0.30(5)	−0.01(5)	$E1$	$\frac{7}{2}^- \rightarrow \frac{7}{2}^+$	338.5
285.8	42(2)	0.55(2)	0.11(2)	−0.51	$\frac{7}{2}^- \rightarrow \frac{5}{2}^-$	338.5
333.0	<1	e			$\frac{11}{2}^- \rightarrow \frac{9}{2}^-$	1013.2
341.7	5(2)	0.51(6)	0.04(8)	−0.47	$\frac{9}{2}^- \rightarrow \frac{7}{2}^-$	680.2
461.6	<1	e			$\frac{13}{2}^- \rightarrow \frac{11}{2}^-$	1474.8
627.5	29(3)	0.33(5)	−16(6)	$E2$	$\frac{9}{2}^- \rightarrow \frac{5}{2}^-$	680.2
630.2	20(2)	−0.55(6)	0.09(7)	0.11	$\frac{11}{2}^+ \rightarrow \frac{9}{2}^+$	768.9
674.7	45(3)	0.37(3)	−0.18(3)	$E2$	$\frac{11}{2}^- \rightarrow \frac{7}{2}^-$	1013.2
691.9	<2	e			$\frac{11}{2}^+ \rightarrow \frac{7}{2}^+$	768.9
741.5	100(2)	0.24(4)	−0.19(5)	$E2$	$\frac{13}{2}^+ \rightarrow \frac{9}{2}^+$	880.2
782.2	3(1)	e			$\frac{15}{2}^+ \rightarrow \frac{13}{2}^+$	1662.3
794.6	37(5)	d		$E2$	$\frac{13}{2}^- \rightarrow \frac{9}{2}^-$	1474.8
816.9	40(5)	0.47(5)	−0.25(5)	$E2$	$\frac{15}{2}^- \rightarrow \frac{11}{2}^-$	1830.1
890.5	<2	e			$\frac{19}{2}^+ \rightarrow \frac{17}{2}^+$	2707.7
893.5	3(1)	e			$\frac{15}{2}^+ \rightarrow \frac{11}{2}^+$	1662.3
912.8	35(4)	0.41(5)	−0.25(6)	$E2$	$\frac{19}{2}^- \rightarrow \frac{15}{2}^-$	2742.9
922.7	28(4)	0.35(3)	−0.17(4)	$E2$	$\frac{17}{2}^- \rightarrow \frac{13}{2}^-$	2397.5
937.0	72(7)	d		$E2$	$\frac{17}{2}^+ \rightarrow \frac{13}{2}^+$	1817.2
949.1	21(4)	0.44(6)	−0.15(7)	$E2$	$\frac{29}{2}^+ \rightarrow \frac{25}{2}^+$	4905.0
976.0	14(4)	0.32(7)	−0.08(7)	$E2$	$\frac{21}{2}^- \rightarrow \frac{17}{2}^-$	3373.5
988.1	9(2)	0.33(6)	−0.05(7)	$E2$	$\frac{23}{2}^- \rightarrow \frac{19}{2}^-$	3731.1
1042.2	27(3)	0.32(4)	−0.17(4)	$E2$	$\frac{25}{2}^+ \rightarrow \frac{21}{2}^+$	3955.9
1045.4	3(1)	e			$\frac{19}{2}^+ \rightarrow \frac{15}{2}^+$	2707.7
1058.0	5(2)	d		$E2$	$\frac{25}{2}^- \rightarrow \frac{21}{2}^-$	4431.5
1096.5	47(5)	0.26(5)	−0.05(6)	$E2$	$\frac{21}{2}^+ \rightarrow \frac{17}{2}^+$	2913.7
1106.3	8(2)	0.30(8)	−0.04(9)	$E2$	$\frac{27}{2}^- \rightarrow \frac{23}{2}^-$	4837.3
1123.6	5(1)	0.27(7)	−0.07(8)	$E2$	$\frac{33}{2}^+ \rightarrow \frac{29}{2}^+$	6028.6
1224.1	<1	e			$\frac{29}{2}^- \rightarrow \frac{25}{2}^-$	5655.7
1239.1	<2	e			$\frac{31}{2}^- \rightarrow \frac{27}{2}^-$	6076.4
1296.2	3(1)	e			$\frac{37}{2}^+ \rightarrow \frac{33}{2}^+$	7324.8
1306.0	<1	e			$\frac{35}{2}^- \rightarrow \frac{31}{2}^-$	7382.4

[a]Intensity in LEPS detector at 0°. Corrected for internal conversion ($\epsilon=6.5$).
[b]Corrected for internal conversion ($\epsilon=12.5$).
[c]Corrected for internal conversion ($\epsilon=0.88$).
[d]Doublet.
[e]Insufficient singles yield.

assignment of the detected γ rays to ^{83}Zr or ^{83}Y, respectively. Table I lists the energies and yields of transitions in ^{83}Zr that were identified in the present reaction and placed in the level scheme.

C. γ-γ coincidences

The γ rays were detected in a Compton suppressed intrinsic Ge detector (25% efficiency) in coincidence with a 27% efficiency Ge(Li) detector. The Compton suppressor is a 152 cm long by 127 cm outer diameter bismuth germanate (BG) annulus which surrounds the Ge detector.[18] The time window of the γ-γ coincidence circuit was 40 ns wide. An additional coincidence was required with a multiplicity filter consisting of two 3×3 in NaI(Tl) detectors. At a target-detector distance of 2.5 cm the NaI detectors covered a very large solid angle of about 5.5 sr (or 44% of 4π). A thick 14 mg/cm^2 target of 95.6% enriched ^{54}Fe was bombarded with a 110 MeV ^{32}S beam. The two parameter coincidence data were recalibrated and subsequently sorted off line into a 2500 channel half diagonal square matrix on a MicroVAX II computer with 16 Mbytes of physical memory. The size of the physical memory is sufficient to hold the entire coincidence matrix which allows a practically instantaneous projection of the gated spectra. Figures 2–4 show the summed coincidence spectra of the three major γ-ray cascades in ^{83}Zr. The individual gates contributing to each spectrum are given in the figures.

D. Delayed γ-γ coincidences

The present reaction was probed for very low energy γ rays and isomeric states in a delayed γ-γ coincidence experiment using a low energy photon spectrometer (LEPS). The 110 MeV ^{32}S beam was stopped in the 14 mg/cm^2 ^{54}Fe target. A planar Aptec germanium x-ray spectrometer with a 0.076 mm thick Be window was positioned at 0° to the beam direction. An additional thin aluminum foil was placed between the 1.27 mm thin Plexiglas wall of the target chamber and the detector to attenuate Fe x rays. A coincidence window of 4 μs between the Compton suppressed γ detector and the x-ray detector was chosen to allow the detection of delayed γ rays. The three parameter coincidence data were sorted off line into several 1500 channel square matrices. Prompt and delayed γ-γ coincidence events were sorted into separate matrices. Two more matrices were constructed containing the γ-TAC (time to amplitude converter) coincidence events of the two Ge detectors, respectively.

Figure 5 shows the LEPS spectrum in coincidence with the 61.7 keV transition, the strongest γ ray in ^{83}Zr previously identified in the recoil-γ and neutron-γ coincidences. This spectrum, obtained by projection from the delayed LEPS-γ matrix, allowed the identification of two delayed transitions of 24.3 and 52.7 keV as part of the decay scheme of ^{83}Zr. Both transitions will be discussed in more detail in Secs. III B and III D.

Internal conversion is a strongly competing decay mode for low energy transitions. The conversion electrons from the decay of the 24.3 and 52.7 keV transitions give rise to x-ray emission. The identification of the Zr K_α and K_β x rays in the coincidence spectrum of Fig. 5 in combination with the recoil-γ and neutron-γ coincidence results provide an unambiguous assignment of the above transitions to ^{83}Zr.

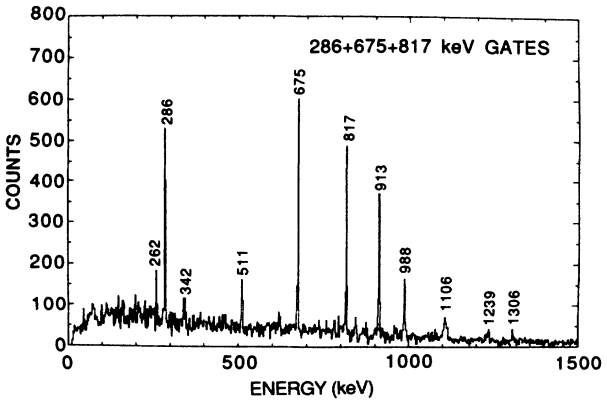

FIG. 3. Summed γ-γ coincidence spectrum from gates on transitions in the negative parity, negative signature band with energies of 286, 675, and 817 keV.

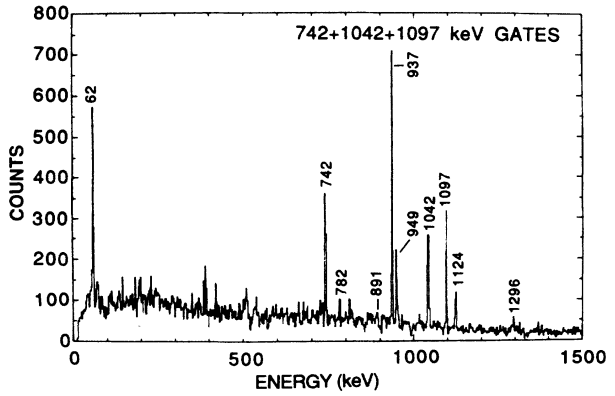

FIG. 2. Summed γ-γ coincidence spectrum from gates on transitions in the positive parity, positive signature band with energies of 742, 1042, and 1096 keV.

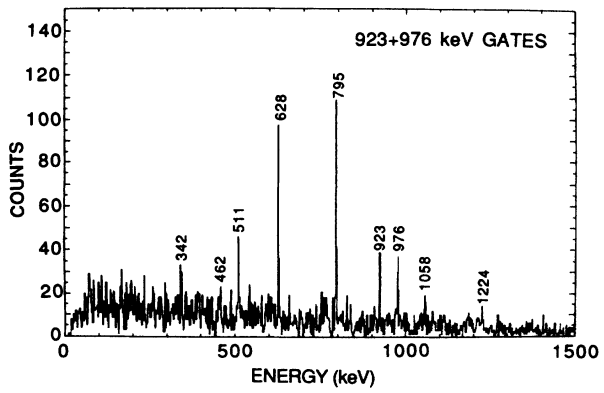

FIG. 4. Summed γ-γ coincidence spectrum from gates on transitions in the negative parity, positive signature band with energies of 923 and 976 keV.

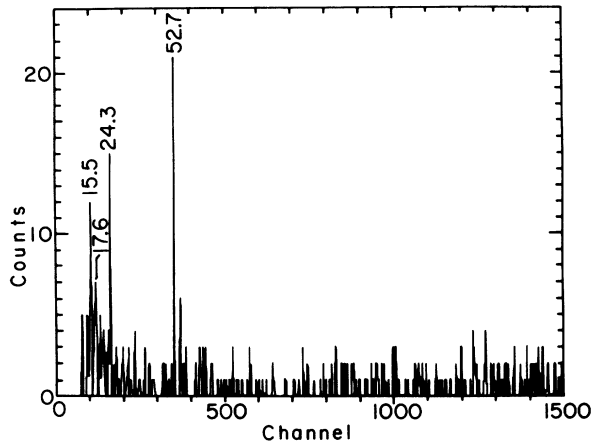

FIG. 5. LEPS spectrum in coincidence with the 61.7 keV transition. The TAC window is 0–2 μs. The 15.5 and 17.6 keV transitions are Zr K_α and K_β x rays, respectively.

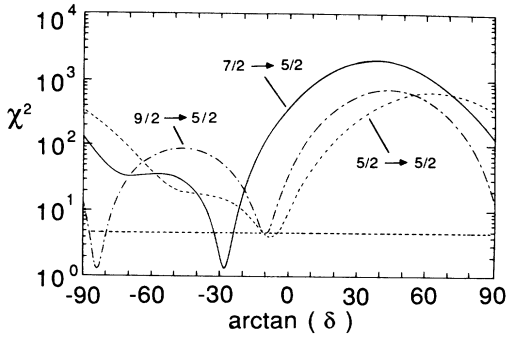

FIG. 6. χ^2 fit of the 285.7 keV transition in ^{83}Zr. The adopted spin of the initial state is $\frac{7}{2}\hbar$ (solid line). The minimum χ^2 is at $\delta=-0.51$, i.e., a multipolarity of $M1+20\%$ $E2$.

E. γ-ray angular distribution measurements

Angular distributions were obtained with a Compton suppressed Ge detector at $\theta_\gamma=0°$, 30°, 45°, 60°, and 90°. At the same time a second analog-to-digital converter (ADC) was gated with a sum multiplicity signal from three NaI detectors to filter out overlapping γ rays from contaminants and β-decay products. The spectra were normalized using both dead-time-corrected beam integration and some of the stronger peaks detected in a Compton suppressed monitor at a fixed position of 90° to the beam direction.

The peak areas from the singles measurements were determined with an iterative code for fitting γ-ray spectra.[19] The reduced angular distribution data were least-squares fitted to the Legendre polynomial expansion

$$W(\theta)=1+A_2P_2(\cos\theta)+A_4P_4(\cos\theta)\ . \quad (1)$$

Practically no discrepancy was found between the results for the pure singles compared to the multiplicity filtered singles data. The A_2 and A_4 coefficients obtained from the latter are given in Table I. A χ^2 analysis was performed, assuming a Gaussian distribution of the magnetic substates.[20] The free parameters are the mixing ratio (δ) and the width of the magnetic substate distribution[21] (σ). The theoretical angular distributions have been shown[22] to vary only slightly in the range of $0\le\sigma\le1.6$. Figure 6 shows some of the χ^2 fits for the 285 keV transition with $\sigma=1.0$. The mixing ratios for mixed $E2/M1$ transitions are given in Table I.

III. DISCUSSION OF THE LEVEL SCHEME

A. The ground state of ^{83}Zr

As pointed out in the Introduction, no information on the level structure of ^{83}Zr was published at the beginning of the present work. At present, even the spin of the ground state is not yet firmly established. Based on the systematics of neighboring nuclei the possibility of a $J^\pi=\frac{5}{2}^-$ assignment for the ground state of ^{83}Zr was pointed out in earlier work.[23] The radioactive decay of ^{83}Zr has previously been studied by several groups. The first reported investigation[6] involved the bombardment of Y with 660 MeV protons, leading to a half-life estimate for the ground state in the range of 5–10 min. In subsequent work, the β decay of ^{83}Zr has been studied following its production in the ^{54}Fe(^{32}S,2pn)^{83}Zr reaction,[7,8,10,11] the ^{58}Ni(^{28}Si,2pn)^{83}Zr reaction,[9] and, recently, following the bombardment of natural Mo foil with a 280 MeV ^{3}He beam.[12] In the previous papers[8–12] a spin and parity of $J^\pi=\frac{1}{2}^-$ was assumed for the ground state of ^{83}Zr. The half-life of the ground state was determined to be $T_{1/2}=0.7\pm0.6$ min (Ref. 7), 42±7 s (Ref. 8), 45±4 s (Ref. 9), 44±2 s (Ref. 10), 37.8±1.1 s (Ref. 11), and 44 s (Ref. 12). A long lived isomeric state was attributed a half-life of 8 s (Ref. 10) while in Ref. 11 a 6.0±1.5 s isomeric state was tentatively assigned a spin and parity of $J^\pi=\frac{7}{2}^+$. The recent investigation by Rapaport *et al.*,[12] however, could not support the existence of a 6 s or 8 s high-spin isomeric state in ^{83}Zr.

The level scheme of ^{83}Zr deduced in the present work is also not consistent with the existence of a long-lived isomeric state. The observation[12] of allowed β decay to a $J^\pi=\frac{3}{2}^-$ isomeric state in ^{83}Y firmly established negative parity for the ground state of ^{83}Zr. This leaves $J^\pi=\frac{1}{2}^-$, $\frac{3}{2}^-$, or $\frac{5}{2}^-$ as candidates for the ground state. In order to obtain some guidance from the neighboring nuclei, Fig. 7 shows the low energy level systematics of the $N=43$ isotones. The ground states of all $N=43$ isotones displayed in Fig. 7 have $J^\pi=\frac{1}{2}^-$. Assuming a $\frac{1}{2}^-$ ground state for ^{83}Zr, the present data establish the spin and parity assignments to the $\frac{5}{2}^-$, $\frac{7}{2}^+$, $\frac{9}{2}^+$, and higher lying states (cf. Secs. III B–E). With this assignment, it follows that the strongest cascade of stretched $E2$ transitions identified in the present work decays to the $J^\pi=\frac{9}{2}^+$ state, which is characteristic for odd nuclei in this mass region. Considering, in particular, the strong similarities between the low energy structures of ^{81}Sr and ^{83}Zr, $J^\pi=\frac{1}{2}^-$ remains the most probable assignment for the ground state of ^{83}Zr.

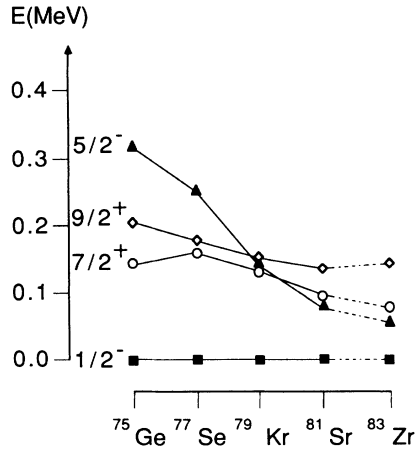

FIG. 7. Low energy systematics of the $N=43$ isotones.

B. The isomeric state at 52.7 keV

The 52.7 keV transition was first observed in the γ singles spectrum and subsequently in the delayed LEPS-γ coincidence experiment. The spectrum projected from the delayed coincidence matrix (100 ns–2 μs) shows that this transition is in coincidence with all the stronger γ rays in ^{83}Zr previously identified by the recoil-γ and neutron-γ coincidence data (Fig. 1), thus allowing an unambiguous assignment of the 52.7 keV transition to ^{83}Zr. The fact that it is the strongest transition (see below) and no other γ transition is found to be in coincidence with the members of all three major γ-ray cascades suggests that the 52.7 keV γ ray is the lowest transition in ^{83}Zr.

The projected TAC spectrum in coincidence with the 52.7 keV transition obtained from the LEPS-γ data was least-squares fitted with an exponential decay curve. The lifetime of the 52.7 keV level determined from the fit is 0.76 ± 0.18 μs.

In order to obtain an estimate of the internal conversion ratio, the spectrum in coincidence with the 674.7 keV transition was projected from the delayed LEPS-γ coincidence matrix. As discussed in Secs. III C and III D, the 338.5 keV level, which is populated by the 674.7 keV transition, can decay directly to the first excited state at 52.7 keV via the 285.8 keV transition, and indirectly via the 261.5 and 24.3 keV transitions. The internal conversion coefficient can be obtained by comparing the intensities of 285.6 and 261.5 keV transitions to the yield of the 52.7 keV transition in the above coincidence spectrum. Depending on the choice of background subtraction gates we found an efficiency corrected intensity ratio of 18 ± 10 and thus an internal conversion coefficient of the same value. The only theoretical conversion coefficients that fall into this range are for $E2$ (12.5) or $M2$ (27.6) transitions. All other multipolarities differ by at least one order of magnitude.

Accounting for the theoretical internal conversion coefficients, the lifetime estimate above leads to an $E2$ transition strength for the 52.7 keV transition of 9.6 Weisskopf single particle units or $B(E2)=211$ e^2fm^4 and an $M2$ transition strength of 275.6 W.u. or $B(M2)=95.6$ e^2fm^4. A comparison of the above transition strengths to the recommended upper limits[24] shows that an $M2$ strength of this magnitude can be ruled out, whereas the $E2$ transition strength is consistent with values generally found in this mass region.

Additional evidence is provided by the necessary intensity balance of transitions decaying to and from the 52.7 keV level. The internal conversion coefficients for electric or magnetic dipole transitions give an insufficient yield of the 52.7 keV transition compared to the sum of the intensities of the 24.3 (or 61.7 + 261.5), 285.8, and 627.5 keV transitions. The $E2$ coefficient, however, raises the relative intensity of the 52.7 keV transition from 31 to a consistent value of about 385. Thus, assuming a $J^\pi=\frac{1}{2}^-$ ground state, the 52.7 keV level is assigned a spin and parity of $J^\pi=\frac{5}{2}^-$.

C. The negative parity bands

The γ rays of the strongest cascade found in coincidence with the 52.7 keV transition have energies (listed in order of decreasing intensity) of 285.8, 674.7, 816.9, 912.8, 988.1, 1106.3, 1239.1, and 1306.0 keV (cf. Fig. 3). A second γ-ray sequence consists of transitions of 627.5, 794.6, 922.7, 976.0, 1058.0, and a 1224.1 keV (cf. Fig. 4).

The 285.8 keV transition is the strongest γ ray among the members of the two cascades. Almost all of the decays to the 52.7 keV, $\frac{5}{2}^-$ bandhead are found in its coincidence gate except for the 627.5 keV and some of the weaker high spin transitions in the second band. The angular distribution of the 285.8 keV transition indicates a $\Delta J=1$ transition and the χ^2 analysis (cf. Fig. 6) suggests a spin assignment of $\frac{7}{2}^-$ for the 338.5 keV level.

This assignment is further supported by the existence of the 341.7 keV interband transition. Its angular distribution is consistent with a $\Delta J=1$ transition. The angular distribution of the 627.5 keV γ ray is consistent with an $E2$ transition and it is not in coincidence with either the 285.8 keV and 341.7 keV transitions. Thus, spin and parity of $\frac{9}{2}^-$ are assigned to the 680.2 keV level. The remaining higher energy transitions of the two bands display angular distributions consistent with stretched $E2$ transitions and the intensity relations suggest the level structure of the negative parity bands shown in Fig. 8. The existence of some weak interband transitions provides additional evidence for the displayed decay scheme.

D. The isomeric 77.0 keV level

A second delayed transition was found in coincidence with transitions of the dominant γ-ray cascade in the course of the analysis of the delayed LEPS-γ coincidence data. At an energy of 24.3 keV this transition could only be observed in the LEPS detector. A lifetime estimate of 190 ± 80 ns for the initial state of the 24.3 keV transition is obtained from the coincident TAC spectrum. The ratio of the efficiency and γ-ray attenuation

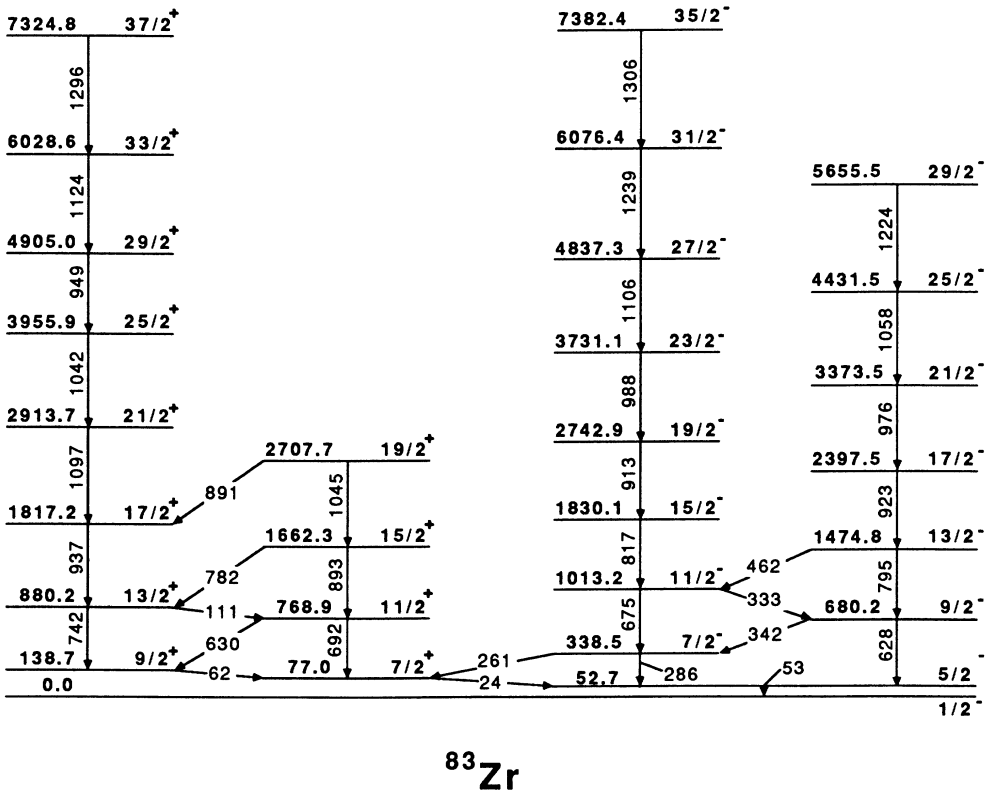

FIG. 8. The level scheme of ^{83}Zr deduced from the present work.

corrected yields of the 52.7 and 24.3 keV peaks in the spectrum in coincidence with the delayed 61.7 keV transition leads to an internal conversion coefficient of 8 ± 4 for the 24.3 keV transition. A comparison to the theoretical conversion coefficient of $E1$ (6.5) and $M1$ (12.4) somewhat favors an $E1$ multipole assignment. The internal conversion coefficients of all higher order multipoles are more than one order of magnitude too large. Transition strengths of the corresponding multipoles were calculated for $E1$ to be 3×10^{-5} W.u. or $B(E1)=4\times10^{-5}\ e^2\text{fm}^2$ and for $M1$ to be 9×10^{-4} W.u. or $B(M1)=5\times10^{-6}\ e^2\text{fm}^2$. The above $E1$ strength is frequently found for $E1$ transitions in the mass 80 region, while the $M1$ strength is on the border of the empirical γ-ray strength distribution curves.[24]

The 24.3 keV γ ray is also observed in the spectrum coincident with the delayed 261.5 keV transition. This γ ray depopulates the 338.5 keV level of the negative parity band as inferred from the coincidence spectra of the 285.8 and 674.7 keV transitions and the intensities of the 674.7 and 341.7 keV γ rays compared to the yield of the 285.8 keV transition. The angular distribution of the 261.5 keV transition is consistent with a $\Delta J=0$ or 2 transition. In combination with the 24.3 keV γ ray a spin and parity assignment of $\frac{7}{2}^+$ to the 77.0 keV level is strongly suggested and both transitions decaying to and from this level are inferred to be of $E1$ type.

E. The positive parity bands

The 77.0 keV $\frac{7}{2}^+$ level is identified as the lowest member of the $g_{9/2}$ yrast band, which consists of the 61.7, 741.5, 937.0, 1096.5, 1042.2, 949.1, 1123.6, and 1296.2 keV transitions, in order of decreasing intensity (cf. Fig. 2). The angular distribution of the 61.7 keV γ ray is consistent with a $\Delta J=1$ transition and suggests a spin assignment of $\frac{9}{2}^+$ for the 139.0 keV level. All other members of this band display angular distribution consistent with stretched $E2$ transitions and the level scheme is readily constructed from the intensity ratios.

Band members of the opposite signature could also be identified from the coincidence data. The 630 keV and 111 keV γ rays are found to be coincident with the 61 keV and the 937 keV transitions. The singles yield of the 630 keV γ ray is sufficient to extract A_2 and A_4 coefficients which are consistent with a $\Delta J=1$ transition.

The 782 keV and 1045 keV γ rays are found to be in coincidence with the 741 keV transition. Their intensities, however, are not sufficient to obtain angular distribution information from the present data. Spin assignments in this case are mainly based on the existence of the 894 keV and 891 keV transitions.

IV. SHAPE TRANSITION AROUND $N=44$ IN THE Sr AND Zr ISOTOPES

Before discussing the high-spin properties of ^{83}Zr, we would like to focus first on the shape changes in neighboring Sr and Zr isotopes. Information about such shape properties of even-even cores, like deformation softness or possible shape coexistence effects, is essential when analyzing data in terms of polarization effects

caused by aligned quasiparticles.

Neutron-deficient Sr isotopes with $N<44$ have very well deformed ground states.[2] These nuclei show very regular rotational bands with large moments of inertia and very fast $B(E2)$ rates. A similar pattern has been observed for the very neutron deficient nuclei ^{80}Zr (Ref. 25) and ^{82}Zr (Ref. 26). With increasing neutron number, however, the collective properties are diminished and isotopes with $N>44$ look more like weakly deformed or spherical vibrators than rotors. Figure 9 shows the collective systematics for the even-even Sr and Zr isotopes with $40\leq N\leq 48$. All quantities displayed in this figure nicely illustrate the effect of the transition from the rotation- to the vibration-like regime. Although this transition looks fairly smooth, it clearly takes place around $N=44$. (The slightly lower collectivity for the $N=42$ systems compared to the $N=40$ isotopes may be due to the interaction with weakly deformed states, see below.) Another striking feature seen in Fig. 9 is that the ground state properties of the Sr and Zr nuclei shown are almost identical.

A summary of the calculated quadrupole deformations is shown in Fig. 10. Since the calculations predict in some cases triaxial local minima in the potential energy surface (PES), the "effective" quadrupole deformation

$$\beta_{2\text{eff}}=\beta_2\frac{\cos(\gamma+30)}{\cos(30)} \tag{2}$$

is displayed rather than the standard deformation parameter β_2. The quantity given by Eq. (2) is closely related to the transition quadrupole moment Q_t. The results presented in Fig. 10 were obtained from three different models:

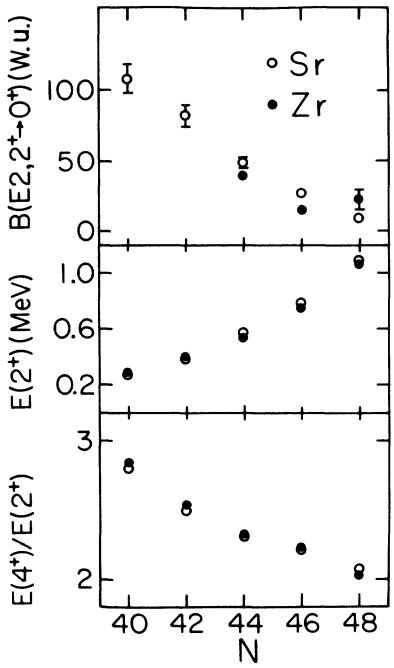

FIG. 9. Collective systematics in the even-even Sr and Zr isotopes as a function of the neutron number N. Experimental data were taken from Refs. 25, 40, and 41 (see also Ref. 42 and references quoted therein).

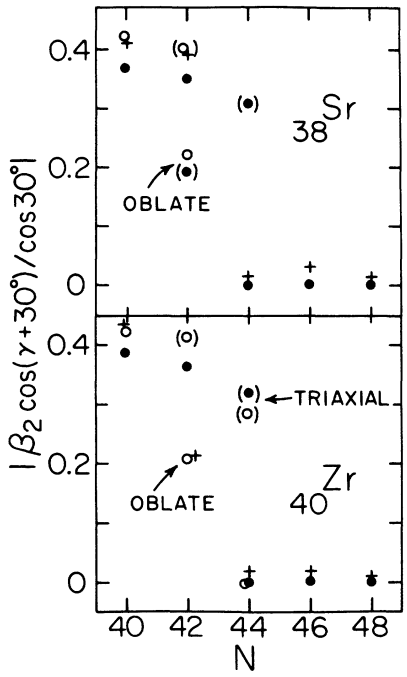

FIG. 10. Theoretical equilibrium quadrupole deformation $\beta_{2\text{eff}}$ [Eq. (2)] for the even-even Sr and Zr isotopes. Results of three theoretical models are presented: the Woods-Saxon model of Ref. 27 (●), the Skyrme III model of Ref. 28 (○), and the folded-Yukawa model of Ref. 29 (+). Symbols in parentheses represent local (excited) energy minima.

(i) The shell correction approach of Ref. 27 based on the Woods-Saxon average potential and the liquid drop macroscopic mass formula.

(ii) The self-consistent Hartree-Fock model of Ref. 28 with the Skyrme III interaction.

(iii) The shell correction approach of Ref. 29 based on the folded-Yukawa average potential and the droplet model macroscopic mass formula.

The results of Fig. 10 can be summarized as follows:

(a) The $N=40$ isotopes are predicted in all models to be prolate deformed with a large quadrupole deformation $\beta_2=0.4$.

(b) The $N=42$ isotopes are predicted to have two or more minima in the PES. The prolate minimum, with $0.35\lesssim\beta_2\lesssim 0.4$, is favored by model (i), but the oblate minimum with $\beta_2\approx 0.2$ is lower in energy in model (ii). Model (iii) predicts ^{80}Sr to have a prolate ground state and ^{83}Zr to be oblate deformed. In fact, both models (i) and (ii) as well as the folded-Yukawa model of Ref. 30 also yield the local spherical minimum in ^{80}Sr and ^{82}Zr. The Skyrme III model predicts in this case an additional well deformed triaxial minimum.

(c) The $N=44$ isotopes are predicted in all three models to have spherical ground states. However, there are also well deformed triaxial minima in the PES of models (i) and (ii).

(d) The $N>46$ isotopes have only one spherical

minimum.

The complex deformation pattern discussed above can qualitatively be understood from the underlying shell structure.[27] On the prolate side the major gaps in the single particle spectrum appear for particle numbers 38 and 40 at a large deformation, $\beta_2 \approx 0.40$. Large spherical and oblate gaps are seen for particle number 40. These gaps are responsible for the low lying weakly deformed configurations in the Zr isotopes. With increasing neutron number the spherical gap at $N=50$ triggers a shape change to the spherical limit.

Theoretically, the transition from the rotation to the vibration-like pattern should take place at $N=44$. The experimental data displayed in Fig. 10 do not show any dramatic change at this neutron number. It is most likely due to the configuration mixing between well deformed prolate or triaxial structures on the one side and weakly deformed oblate or spherical structures on the other side. Such a low spin mixing is a well established phenomenon seen experimentally in the lighter Se and Kr nuclei (see, e.g., discussions in Refs. 27 and 31). At higher angular momenta, however, the shape of the nucleus is expected to be stabilized at a well deformed shape due to an associated large moment of inertia.[31]

One can thus expect that the $N=43$ nuclei ^{81}Sr and ^{83}Zr, having γ- and β-soft cores, should be very sensitive to all the effects which are associated with shape changes and shape polarization. In principle, one may expect different rotational bands built on prolate, triaxial, and oblate shapes to coexist, depending on the geometrical properties of the odd neutron. At higher spins other shape changes are expected due to the progressing quasiparticle alignment.

V. ANGULAR MOMENTUM ALIGNMENT IN ^{83}Zr

In order to analyze the angular momentum alignment in ^{83}Zr and in neighboring nuclei, the cranked shell model (CSM) of Ref. 32 has been employed. The results of the CSM calculations are shown in Figs. 11–13. Because of the pronounced shape effects it is very difficult to choose a reasonable set of reference parameters J_0 and J_1 describing the smooth rotational behavior of the even-even vacuum configuration. Our reference parameters $J_0=15\hbar^2/\text{MeV}$ and $J_1=4\hbar^4/\text{MeV}^3$ can thus be regarded as a compromise to allow the presentation of all the data for the bands discussed on the same graph.

The aligned angular momenta (i) for the positive parity, even-spin ($\pi=+$, $\alpha=0$) yrast bands in ^{82}Zr and ^{84}Zr and for both negative parity bands in ^{83}Zr are displayed in the top part of Fig. 11. At low spins the negative parity bands carry quite a sizable amount of angular momentum, about $2\hbar$. At a frequency of $\hbar\omega \approx 0.48$ MeV, a very similar gradual increase in angular momentum is seen in the data for ^{83}Zr and ^{84}Zr. In order to emphasize this similarity we plotted the second moment of inertia, $J^{(2)}$ in the bottom part of Fig. 11. Both $\pi=-$ bands in ^{83}Zr and the $\pi=+$ yrast band in ^{84}Zr display a gentle upbending at the same frequency which shows up as the peak in the second moment of inertia. In Ref. 5 this upbending in ^{84}Zr has been interpreted in terms of a band crossing associated with the alignment of a pair of

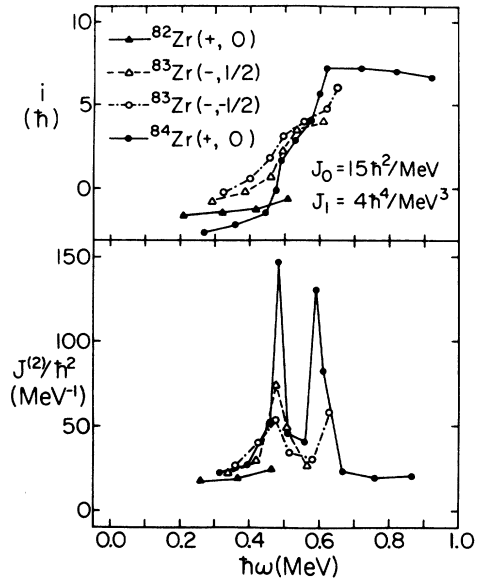

FIG. 11. Aligned angular momentum (top) and second moment of inertia (bottom) for $\pi=-$ bands in ^{83}Zr and $\pi=+$ yrast bands in ^{82}Zr (Ref. 26) and ^{84}Zr (Ref. 4).

$g_{9/2}$ protons. The total alignment gain in the negative parity bands in ^{83}Zr is about $4.5\hbar$ which is only slightly less than the corresponding value for ^{84}Zr, $i=5\hbar$.

The next crossing in the yrast band of ^{84}Zr can be seen at $\hbar\omega=0.59$ MeV. It is most likely due to the alignment of a pair of $g_{9/2}$ neutrons.[4] The same crossing is present in the negative parity bands in ^{83}Zr. On the basis of the present data one may give an approximate value of $\hbar\omega=0.63$ MeV for this crossing.

The positive parity favored $g_{9/2}$ band ($\pi=+$, $\alpha=\frac{1}{2}$) in ^{83}Zr shows a sharp backbending at $\hbar\omega \approx 0.51$ MeV (cf. Fig. 12). The associated gain in angular momentum is about $5.5\hbar$. This sharp band crossing must be due to the alignment of a pair of $g_{9/2}$ protons, since the $g_{9/2}$ neutron orbital is blocked. The very small value of the band interaction and the large value of the angular momentum alignment in this band, as compared to the negative

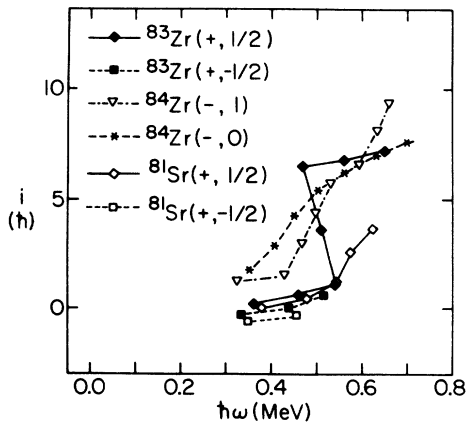

FIG. 12. Aligned angular momentum for both $g_{9/2}$ bands in ^{83}Zr, the negative parity bands in ^{84}Zr (Ref. 4) and the $g_{9/2}$ bands in ^{81}Sr.

parity bands, suggest that there must be a structural difference between the $g_{9/2}$ proton alignment processes in these bands.

The angular momentum alignments of the positive parity bands in ^{81}Sr and ^{83}Zr are also compared in Fig. 12. Although the one-quasiparticle alignment is somewhat smaller in ^{81}Sr, these bands are very similar at low frequencies. The experimental data extend beyond the first crossings only for the favored bands and show considerable differences for the three-quasiparticle configurations. The upbend at the first proton crossing in ^{81}Sr indicates a much stronger interaction between the one- and three-quasiparticle bands compared to ^{83}Zr. The gain in angular momentum alignment is only about $2.5\hbar$, less than half the value of ^{83}Zr.

Figure 13 shows the experimental Routhians for the four yrast bands of both parities and signatures in ^{81}Sr and ^{83}Zr. Before the proton crossing, i.e., for $\hbar\omega \leq 0.5$ MeV, the one-quasiparticle $g_{9/2}$ bands look very similar in both nuclei. It can only be noted that the neutron $g_{9/2}$ signature splitting is slightly larger in ^{81}Sr. However, the three-quasiparticle bands differ markedly. At a frequency of $\hbar\omega \approx 0.65$ MeV, the $(\pi,\alpha)=(+,\frac{1}{2})$ band in ^{83}Zr lies about 600 keV below the corresponding band in ^{81}Sr and the difference in alignment is about $3\hbar$ (cf. Fig. 12). There are also differences between the negative parity bands in ^{81}Sr and ^{83}Zr [Fig. 13(b)]. In both nuclei the

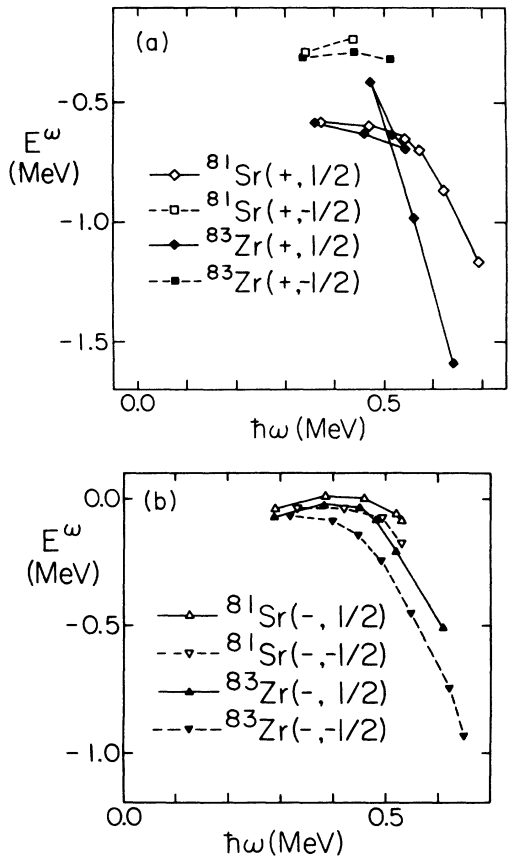

FIG. 13. Experimental quasiparticle excitation energies in a rotating intrinsic system (Routhians) for (a) the positive parity and (b) the negative parity yrast bands in ^{81}Sr (Refs. 38 and 43) and ^{83}Zr.

$(-,-\frac{1}{2})$ band lies lower in energy than the $(-,\frac{1}{2})$ band. The associated signature splitting in ^{83}Zr is about twice as large as in ^{81}Sr. Moreover, the $\pi=-$ bands in ^{83}Zr carry more angular momentum than the corresponding bands in ^{81}Sr. These differences may reflect distinct properties of the even-even cores. According to the Woods-Saxon model results shown in Fig. 10, the core of ^{81}Sr should favor near-prolate and near-oblate configurations, while in ^{83}Zr strongly triaxial shapes are expected. The influence of deformation on the signature splitting and quasiparticle alignment will be discussed in Sec. VI.

The present experimental data for ^{83}Zr brings new light to the structure of the negative parity side bands in ^{84}Zr shown in Fig. 12. Experimentally, up to $\hbar\omega=0.5$ MeV, the $(-,1)$ band in ^{84}Zr lies lower in energy. Based on this argument it has been suggested in Ref. 5 that both negative parity bands in ^{84}Zr must have a proton character. This hypothesis is fully consistent with the results shown in Fig. 13. The lowest negative parity Routhian in ^{83}Zr has the signature $\alpha=-\frac{1}{2}$, which, after combining it with the favored signature of the $g_{9/2}$ neutron, $\alpha=\frac{1}{2}$, would give the total signature $\alpha=0$ for the lowest two-quasiparticle neutron excitation in ^{84}Zr. On the other hand, both the cranking calculations of Ref. 5 (see also Sec. VI) and the experimental data on ^{83}Y (Refs. 33 and 34) indicate that the lowest negative parity Routhian in the proton system has $\alpha=\frac{1}{2}$, which, after combining it with the $\alpha=\frac{1}{2}$ Routhian for the $g_{9/2}$ proton leads to the total signature $\alpha=1$, in full agreement with the experimental findings for ^{84}Zr.

VI. THEORETICAL ANALYSIS

A theoretical analysis of the high spin properties of ^{83}Zr has been carried out using the Woods-Saxon cranking model of Ref. 27. The deformation space was defined using quadrupole deformations β_2 and γ and hexadecapole deformation β_4. The full deformation grid consists of three (β_2,γ) planes of dimension 9×8 corresponding to the different values of β_4 in the deformation space $(\tilde{\beta})$. The main difference between the approach of Ref. 27 and the present model lies in the treatment of the pairing correlations. The pairing force was assumed to be of monopole type. Pairing strengths have been taken into account according to Ref. 27. At zero rotational frequency the Bardeen-Cooper-Schrieffer (BCS) equations were solved for neutrons and protons at each deformation point and the self-consistent pairing gap, Δ(BCS), was determined. At high spins only the particle number equation was solved in order to determine the value of the Fermi level. For the pairing gap the following ansatz was used:

$$\Delta(\omega)=\begin{cases}\Delta(\mathrm{BCS})\left[1-\frac{1}{2}\left[\frac{\omega}{\omega_{\mathrm{crit}}}\right]^2\right], & \omega<\omega_{\mathrm{crit}}\\ \Delta(\mathrm{BCS})\frac{1}{2}\left[\frac{\omega_{\mathrm{crit}}}{\omega}\right]^2, & \omega>\omega_{\mathrm{crit}}\end{cases} \quad (3)$$

where $\omega_{crit}=0.7$ MeV for both neutrons and protons.

The total Routhian $E^{\omega}(N,Z,\tilde{\beta},\omega)$ was subsequently calculated for each quasiparticle configuration ν:

$$E^{\omega}_{\nu}(N,Z,\tilde{\beta},\omega)=E_{\text{Strut}}(N,Z,\tilde{\beta})+E_{\text{rot}}(\nu,N,Z,\tilde{\beta},\omega)\ , \tag{4}$$

where $E_{\text{Strut}}(N,Z,\tilde{\beta})$ is the Strutinsky energy at $I=0$, and $E_{\text{rot}}(\nu,N,Z,\tilde{\beta},\omega)$ represents the rotational energy given by the cranking quasiparticle approach. At a fixed value of the rotational frequency the total Routhian surface (TRS) was found by minimizing E^{ω}_{ν} at each (β_2,γ) grid point with respect to β_4. A detailed description of these calculations will be given in a separate paper.[35] Recently this approach was applied to the case of ^{77}Kr (Ref. 36) where additional references can be found.

In order to get some idea about the single-particle level structure of ^{83}Zr the deformations and energies of the lowest one-quasiparticle bandheads were calculated. Only axial shapes were considered in these calculations. The shapes were defined by means of the deformation parameters (β_2,β_4). In the bandhead calculations the blocked Lipkin-Nogami approach in the realization of Ref. 37 was employed.

The ground state of ^{83}Zr was calculated to be the $g_{9/2}$, $K=\frac{5}{2}$ orbital. It polarizes the core towards an oblate shape with $\beta_2=-0.21$, $\beta_4=-0.03$. Other $g_{9/2}$ orbitals, corresponding to nearly spherical shapes, with $k=\frac{1}{2}$, $\frac{3}{2}$, $\frac{7}{2}$, and $\frac{9}{2}$, were found to be very low in energy. The lowest negative parity bandhead was predicted to be the $K=\frac{1}{2}$ state at an excitation energy of about 150 keV and $\beta_2=-0.13$. This orbital originates from the $p_{1/2}$ subshell, but its wave function also contains large components of the $f_{5/2}$ and $p_{3/2}$ orbitals. At slightly higher energies (about 400 keV) two bandheads were found: $[303]\frac{5}{2}$ and $[301]\frac{3}{2}$. They can be associated with large prolate deformation: $\beta_2=0.26$ and $\beta_2=0.34$, respectively. Experimentally, the ground state of ^{83}Zr has $I^{\pi}=\frac{1}{2}^-$, but the strongly decoupled $g_{9/2}$ band is very close in energy (77 keV, cf. Fig. 8). By comparing the low spin part of the ^{83}Zr level scheme with ^{81}Sr (Ref. 38), one can assign the $I^{\pi}=\frac{5}{2}^-$ state at an excitation energy of 53 keV to the $[303]\frac{5}{2}$ Nilsson state. However, the signature splitting seen in the rotational band built on this state (cf. Fig. 12) suggests that it contains an admixture of the $K=\frac{1}{2}$ and $K=\frac{3}{2}$ Nilsson orbitals.

The total Routhian surfaces for selected quasiparticle configurations in ^{83}Zr are shown in Fig. 14. At low rotational frequencies the TRS are very soft with respect to γ deformation, and the actual minima correspond to triaxial shapes with $\beta_2\approx 0.30$ and $-30^\circ\lesssim\gamma\lesssim-20^\circ$. The TRS at $\hbar\omega=0.3$ MeV for the favored $g_{9/2}$ band and the $(-,\frac{1}{2})$ band are very similar to the ones shown in Figs. 14(a) and 14(b), respectively. The quasiparticle diagram representative for the one-quasiparticle configuration is given in Fig. 15. At this deformation the protons align first at $\hbar\omega\approx 0.45$ MeV in good agreement with the experimental data displayed in Figs. 11 and 12. The $g_{9/2}$ neutron crossing is expected to occur at $\hbar\omega=0.55$ MeV.

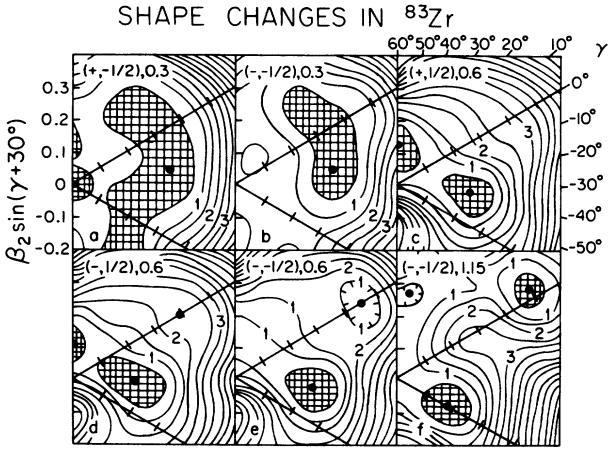

FIG. 14. Total Routhian surfaces (with pairing) in the (β_2,γ) plane for various quasiparticle configurations in ^{83}Zr. Quasiparticle configurations are labeled using the parity and signature quantum numbers (π,α). The numbers give values of rotational frequency (in MeV). The distance between contour lines is 1 MeV. The closed circles show the location of the Routhian minima.

In the quasiparticle diagrams of Figs. 15–18, the prescription for the TRS calculations [given by Eq. (4)] was also used for the effective pairing gap. It should be pointed out that the crossing frequencies estimated from our diagrams will therefore be slightly underestimated compared to those obtained using the fixed pairing gap prescription.

The aligned pair of the $g_{9/2}$ protons induces a shape polarization towards smaller values of β_2 and slightly more negative values of γ (Ref. 31). This is clearly seen in Figs. 14(c)–14(e) which present TRS at a frequency of $\hbar\omega=0.6$ MeV, i.e., after the proton crossing. The absolute minima can be associated with well developed triaxial shapes with $\beta_2\approx 0.22$ and $\gamma\approx-33^\circ$. At this shape the quasiparticle alignment of $g_{9/2}$ particles is markedly increased, see Fig. 16. In both Figs. 15 and 16 the first

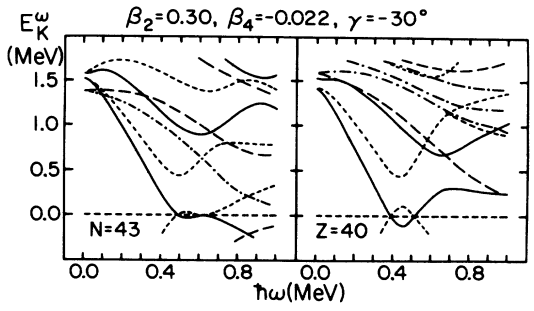

FIG. 15. Quasiparticle Routhians for ^{83}Zr at a deformation $\beta_2=0.30$, $\beta_4=0.022$, and $\gamma=-30^\circ$, characteristic of one-quasiparticle bands. The spin and parity of Routhians are indicated in the following way: $(+,\frac{1}{2})$, full line; $(+,-\frac{1}{2})$, short-dashed line; $(-,\frac{1}{2})$, long-dashed line; $(-,-\frac{1}{2})$, dot-dashed line. The pairing gap was assumed to be a smooth function of rotational frequency given by Eq. (3).

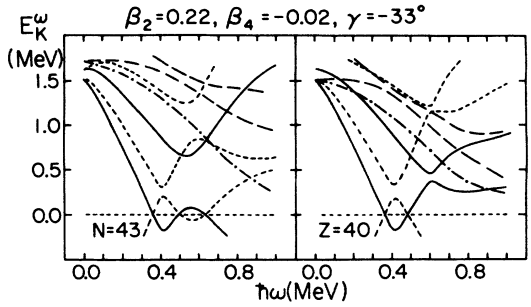

FIG. 16. Similar to Fig. 15, but at a deformation of $\beta_2=0.22$, $\beta_4=-0.02$, and $\gamma=-33°$, typical of three-quasiparticle bands.

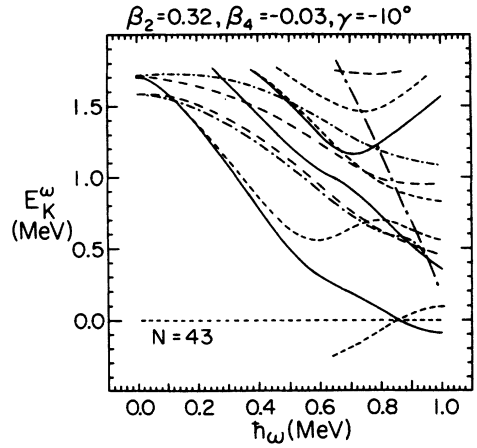

FIG. 18. Similar to Fig. 15, but at a deformation of $\beta_2=0.32$, $\beta_4=-0.03$, and $\gamma=-10°$, representative for the negative parity one-quasiparticle bands in ^{81}Sr.

neutron crossing in the $g_{9/2}$ band (the so called *BC* crossing) has a very large band interaction which would lead to a very smooth, gradual angular momentum alignment in the three-quasiparticle positive parity bands.

A very well deformed near-prolate minimum with $0.4\lesssim\beta_2\lesssim0.5$ can be seen in Figs. 14(d) and 14(e). It is already very low in energy for the $(-,-\frac{1}{2})$ band at $\hbar\omega=0.6$ MeV and becomes yrast at higher frequencies, see Fig. 14(f). The reason for a low lying minimum at this particular configuration is clearly seen from Fig. 17. The lowest $h_{11/2}$ orbital with signature $\alpha=-\frac{1}{2}$ approaches the Fermi surface at larger prolate deformations and quickly becomes occupied; at $\beta_2=0.5$, $\gamma=0°$, the $[550]\frac{1}{2}$ level becomes the lowest $\pi=-$ one-quasiparticle excitation for $N=43$. One may expect to see experimentally this well deformed intruder at high spins. Well deformed prolate minima are in fact predicted for all configurations discussed. However, the one which corresponds to the $(-,-\frac{1}{2})$ configuration lies particularly low in energy.

The predicted deformation changes in ^{83}Zr are consistent with the polarization effects in ^{84}Zr discussed in Ref. 5. At low spins, this nucleus was predicted to be triaxial with $-30°\lesssim\gamma\lesssim-20°$ and consecutive proton and neutron $g_{9/2}$ alignments are expected to drive the nuclear shape towards smaller β_2 deformations and more negative γ values. The well deformed near prolate "$h_{11/2}$" bands with $\beta_2\approx0.5$ were calculated to become yrast at high spins ($I\gtrsim35\hbar$). This very similar deformation pattern, as well as the similarity between the experimental data for ^{84}Zr and ^{83}Zr discussed in connection with Fig. 11, suggest that at least the negative parity bands in ^{83}Zr can be treated as coupled to the ^{84}Zr core.

Finally, we would like to make a comment on the difference in signature splitting for the $\pi=-$ band in ^{81}Sr and ^{83}Zr (cf. Fig. 12). Calculations for ^{81}Sr indicate that negative parity bands can be associated with near-prolate shapes with $\beta_2\approx0.32$, $\gamma\approx-10°$. At this deformation the lowest negative parity Routhian still has the signature $\alpha=-\frac{1}{2}$, but the signature splitting is considerably reduced (cf. Fig. 18). For a detailed discussion of the high-spin properties of ^{81}Sr the reader is referred to a separate paper.[39]

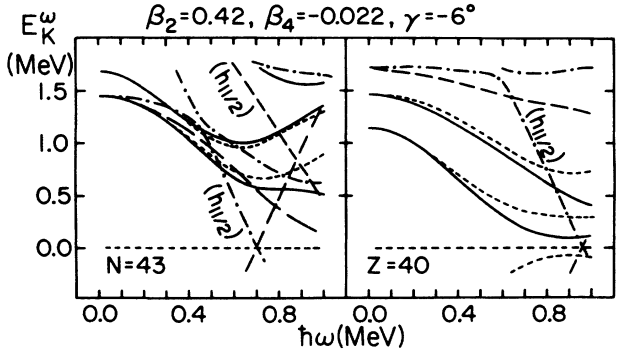

FIG. 17. Similar to Fig. 15, but at a deformation of $\beta_2=0.42$, $\beta_4=-0.022$, and $\gamma=-6°$, typical to the well deformed prolate minimum of Fig. 14. Note that at $\hbar\omega>0.5$ MeV the lowest $(-,-\frac{1}{2})$ excitation corresponds to the occupation of the $h_{11/2}$ orbital.

VII. CONCLUSIONS

The present work presents, for the first time, the yrast level scheme of ^{83}Zr. The combination of recoil-γ, neutron-γ, and x-ray-γ coincidences allowed an unambiguous identification of γ rays from the decay of excited states in ^{83}Zr. Based on Compton suppressed and multiplicity filtered γ-γ coincidences, the observed transitions could be grouped into essentially four rotational bands extending to high spins. The low energy level scheme was determined from the results of a delayed LEPS-γ coincidence experiment. From the latter experiment two low-lying isomeric states were identified and their lifetimes were measured. The spin assignments were based on angular distribution measurements and, in the case of the short-lived isomeric states, on lifetime information

and experimental internal conversion ratios.

The positive parity band displays the characteristics of a rotation-aligned band built on the odd $g_{9/2}$ neutron configuration. This band was observed up to spin $\frac{37}{2}\hbar$ with the first band crossing, due to the alignment of a pair of $g_{9/2}$ protons, showing a sharp backbend at $\hbar\omega=0.5$ MeV. A strongly coupled negative parity band based on a $J^{\pi}=\frac{5}{2}^{-}$ bandhead was observed up to spin $\frac{35}{2}\hbar$. A gradual increase in angular momentum alignment is observed at a frequency of $\hbar\omega\approx 0.48$ MeV. The similar upbend in the ^{84}Zr core suggests a band crossing associated with the alignment of a pair of $g_{9/2}$ protons.

The existence of a 6.0 ± 1.5 s isomeric $\frac{7}{2}^{+}$ state suggested in Ref. 11 could not be confirmed. We found that in the neutron deficient $N=43$ isotones ^{81}Sr (Ref. 38) and ^{83}Zr the $\frac{7}{2}^{+}$ level lies energetically above the $\frac{5}{2}^{-}$ level. In the present work the γ decay from the $\frac{7}{2}^{+}$ state to the $\frac{5}{2}^{-}$ state was observed and the lifetime of the $\frac{7}{2}^{+}$ level was estimated to be 190 ± 80 ns. This is supported by the results of a recent investigation[12] where no isomeric state with a half-life of $1\text{ s}<T_{1/2}<44$ s was observed in ^{83}Zr. The trend of increasing $B(E2;\ \frac{5}{2}^{-}\rightarrow\frac{1}{2}^{-})$ values for the $N=43$ isotones, previously observed in Ref. 23, was found to continue from 2.1 W.u. in ^{77}Se, 3.5 W.u. in ^{79}Kr, and 7.5 W.u. in ^{81}Sr to 9.6 W.u. in ^{83}Zr.

A theoretical analysis was performed using the Woods-Saxon cranking model. The low frequency structure is associated with strongly deformed triaxial shapes that are very soft with respect to γ deformation. After the first crossing the aligned pair of $g_{9/2}$ protons induces a shape polarization towards smaller deformation and well developed triaxial shapes. At very high spins well deformed prolate configurations are predicted by the calculations. The well deformed $(-,-\frac{1}{2})$ intruder band with the lowest $\nu h_{11/2}$ orbital occupied is expected to appear very close to yrast already at $\hbar\omega\approx 0.6$ MeV (cf. Fig. 14).

There is an interesting similarity between the low energy structure of the even-even Sr and Zr isotopes. This systematic trend also holds true for the one-quasiparticle configurations in ^{81}Sr and ^{83}Zr. Some of the transition energies between corresponding levels at low excitation energy even agree to the nearest keV. Adding a pair of protons to the $Z=38$ configuration seems to have very little effect on the low energy structure. One has to note, however, that the signature splitting seen in the negative parity bands in ^{83}Zr is about twice as large as in ^{81}Sr. The three-quasiparticle configurations, on the other hand, are markedly different. The sharp backbend at the first crossing in the positive parity band of ^{83}Zr does not have its analogy in the corresponding band in ^{81}Sr. Our calculations suggest that the negative parity bands in ^{83}Zr can be associated with stronger triaxial deformation compared to the corresponding bands in ^{81}Sr.

ACKNOWLEDGMENTS

This work was supported in part by the U.S. National Science Foundation. One of us (W.N.) was also supported by the Florida State University Supercomputer Computations Research Institute which is partially funded by the U.S. Department of Energy through Contract No. DE-FC05-85ER250000, and by the Polish Ministry of Science and Higher Education through Contract CPBP 01.09.

*Present address: Chemistry Department, Eastern Mennonite College, Harrisonburg, VA 22801.

[1] R. B. Piercey, J. Hamilton, R. Soundranayagam, A. V. Ramayya, C. F. Maguire, X.-J. Sun, Z. Z. Zhao, R. L. Robinson, H. J. Kim, S. Frauendorf, J. Döring, L. Funke, G. Winter, J. Roth, L. Cleemann, J. Eberth, W. Neumann, J. C. Wells, J. Lin, A. C. Rester, and H. K. Carter, Phys. Rev. Lett. **47**, 1514 (1981).

[2] C. J. Lister, B. J. Varley, H. G. Price, and J. W. Olness, Phys. Rev. Lett. **49**, 308 (1982).

[3] C. J. Lister, W. Gelletly, B. J. Varley, H. G. Price, and J. W. Olness, in *Proceedings of the International Conference on Nuclear Physics with Heavy Ions,* Stony Brook, New York, 1983, Vol. VI of *Nuclear Science Research Conference Series,* edited by P. Braun-Munzinger (Harwood Academic, New York, 1984).

[4] H. G. Price, C. J. Lister, B. J. Varley, W. Gelletly, and J. W. Olness, Phys. Rev. Lett. **51**, 1842 (1983).

[5] J. Dudek, W. Nazarewicz, and N. Rowley, Phys. Rev. C **35**, 1489 (1987).

[6] N. G. Zaitseva, V. V. Kuznetsov, M. Ya. Kuznetsova, Ma Ho Ik, G. Musiol, Han Shu-Jun, Chou Mo-Ling, and V. G. Chumin, Yad. Fiz. **1**, 385 (1965) [Sov. J. Nucl. Phys. **1**, 273 (1965)].

[7] T. A. Doron and M. Blann, Nucl. Phys. **A161**, 12 (1971).

[8] M. Kaba and K. Miyano, Radiochim. Acta **21**, 203 (1974).

[9] P. E. Haustein, C. J. Lister, D. E. Alburger, J. W. Olness, and S. Saha, in *Proceedings of the 4th International Conference on Nuclei far from Stability, Helsingør, Denmark, 1981,* edited by P. G. Hansen and O. B. Nielsen (CERN, Geneva, 1981), p. 407.

[10] S. Della-Negra, H. Gauvin. D. Jacquet and Y. Le Beyec, Z. Phys. A **307**, 305 (1982).

[11] E. Hagberg, J. C. Hardy, H. Schmeing, E. T. H. Clifford, and V. T. Koslowsky, Nucl. Phys. **A395**, 152 (1983).

[12] M. S. Rapaport, C. F. Liang, and P. Paris, Phys. Rev. C **36**, 303 (1987).

[13] A. V. Ramayya, M. A. Herath-Banda, W.-C. Ma, N. Schmal, L. Cleemann, J. Eberth, T. Heck, J. Roth, W. König, and B. Martin, Vanderbilt University report, 1983.

[14] U. J. Hüttmeier, C. J. Gross, D. M. Headly, E. F. Moore, S. L. Tabor, P. M. Stwertka, T. M. Cormier, and W. Nazarewicz, Bull. Am. Phys. Soc. **32**, 1079 (1987); Poster Presentation at the Workshop on the Collective Properties of Mid-Mass Nuclei, Tallahassee, 1987.

[15] K. R. Chapman, Nucl. Instrum. Methods **205**, 69 (1983).

[16] T. M. Cormier and P. M. Stwertka, Nucl. Instrum. Methods **184**, 423 (1981).

[17] F. Pühlhofer, Nucl. Phys. A **280**, 267 (1977).

[18] S. L. Tabor, Nucl. Instrum. Methods **B24/25**, 1031 (1987).

[19] R. L. Coldwell, Nucl. Instrum. Methods A **242**, 455 (1986).

[20] R. M. Diamond, E. Matthias, J. O. Newton, and F. S. Stephens, Phys. Rev. Lett. **16**, 1205 (1966).

[21] H. J. Rose and D. M. Brink, Rev. Mod. Phys. **19**, 306 (1967).

[22]P. Taras and B. Haas, Nucl. Instrum. Methods **123**, 73 (1975).
[23]C. J. Lister, P. E. Haustein, D. E. Alburger, and J. W. Olness, Phys. Rev. C **24**, 260 (1981).
[24]P. M. Endt, At. Data Nucl. Data Tables **23**, 547 (1979).
[25]C. J. Lister (unpublished).
[26]B. J. Varley, C. J. Lister, A. J. Irving, H. G. Price, and J. W. Olness, in *Proceedings of the International Conference on High Angular Momentum Properties of Nuclei,* Oak Ridge, 1982, edited by N. R. Johnson (Harwood, New York, 1982), p. 64.
[27]W. Nazarewicz, J. Dudek, R. Bengtsson, T. Bengtsson, and I. Ragnarsson, Nucl. Phys. **A435**, 397 (1985).
[28]P. Bonche, H. Flocard, P. H. Heenen, S. J. Krieger, and M. S. Weiss, Nucl. Phys. **A443**, 39 (1985).
[29]P. Möller, W. D. Myers, W. J. Swiatechki, and J. Treiner, submitted to At. Data Nucl. Data Tables.
[30]R. Bengtsson, P. Möller, J. R. Nix, and J-y. Zhang, Phys. Scr. **29**, 402 (1984).
[31]R. Bengtsson and W. Nazarewicz, in Proceedings of the XIX Winter School Selected Topics in Nuclear Structure, Zakopane, Poland, 1984, edited by Z. Stachura (Raport IFJ No. 1268/PL), p. 171; University of Lund Report No. Lund-MPh-84/09, 1984 (unpublished).
[32]R. Bengtsson and S. Frauendorf, Nucl. Phys. **327**, 139 (1979); **A314**, 27 (1979).
[33]C. J. Lister, private communication.
[34]U. J. Hüttmeier, C. J. Gross, D. M. Headly, E. F. Moore, S. L. Tabor, T. M. Cormier, and P. M. Stwertka, Bull. Am. Phys. Soc. **31**, 64 (1986).
[35]W. Nazarewicz, G. A. Leander, and S. L. Tabor (unpublished).
[36]C. J. Gross, P. D. Cottle, D. M. Headly, U. J. Hüttmeier, E. F. Moore, S. L. Tabor, and W. Nazarewicz, submitted to Phys. Rev. C **36**, 2601 (1987).
[37]W. Nazarewicz, G. A. Leander, P. Quentin, and J. Dudek, Niels Bohr Centennial Symposium on Nuclear Structure, Abstracts, Copenhagen, 1985, p. 91.
[38]S. E. Arnell, C. Ekstrom, L. P. Ekstrom, A. Nilsson, I. Ragnarsson, P. J. Smith, and E. Wallander, J. Phys. G **9**, 1217 (1983).
[39]E. F. Moore, C. J. Gross, P. D. Cottle, D. M. Headly, U. J. Hüttmeier, S. L. Tabor, and W. Nazarewicz (unpublished).
[40]E. K. Warburton, J. W. Olness, C. J. Lister, R. W. Zurmühle, and J. A. Becker, Phys. Rev. C **31**, 1184 (1985).
[41]S. Raman, C. H. Malarkey, W. T. Milner, C. W. Nestor, and P. H. Stelson, At. Data Nucl. Data Tables **36**, 1 (1987).
[42]S. L. Tabor, Phys. Rev. C **34**, 311 (1986).
[43]G. C. Hicks, C. J. Gross, U. J. Hüttmeier, Xi-Ting Lu, G. Neuschaefer, and S. L. Tabor, Phys. Rev. C **29**, 1345 (1984).